CH-Stretching Overtone Spectroscopy of 1,1,1,2-Tetrafluoroethane

Brian G. Saar, Adam H. Steeves,† and John W. Thoman, Jr.*

Department of Chemistry, Williams College, Williamstown, Massachusetts 01267

Daryl L. Howard, Daniel P. Schofield, and Henrik G. Kjaergaard

Department of Chemistry, University of Otago, P.O. Box 56, Dunedin, New Zealand

Received: February 21, 2005

We have recorded the vibrational absorption spectrum of 1,1,1,2-tetrafluoroethane (HFC-134a) in the fundamental and first five CH-stretching overtone regions with the use of Fourier transform infrared, dispersive long-path, intracavity laser photoacoustic, and cavity ringdown spectroscopies. We compare our measured total oscillator strengths in each region with intensities calculated using an anharmonic oscillator local mode model. We calculate intensities with 1D, 2D, and 3D Hamiltonians, including one or two CH stretches and two CH stretches with the HCH bending mode, respectively. The dipole moment function is calculated ab initio with self-consistent-field Hartree−Fock and density functional theories combined with double- and triple-ζ-quality basis sets. We find that the basis set choice affects the total intensity more than the choice of the Hamiltonian. We achieve agreement between the calculated and measured total intensities of approximately a factor of 2 or better for the fundamental and first five overtones.

I. Introduction

In the past decade, hydrofluorocarbons (HFCs) have been considered as replacements for ozone-depleting chlorofluorocarbons (CFCs)[1] and are now commonly used as fire suppressants, refrigerants, and aerosol propellants.[2] Their high heat capacity, low toxicity, and high vapor pressure at room temperature make HFCs ideal for these applications. HFCs differ from CFCs in that they contain one or more CH bonds. The lack of a CH bond in CFCs makes them more inert to atmospheric breakdown, and large fractions of the emitted CFCs survive into the stratosphere. In the stratosphere, ultraviolet photons dissociate the CFCs, producing highly reactive chlorine radicals that cause ozone depletion.[3] These undesirable reactions have led to the search for CFC-replacement compounds such as HFCs. HFCs react with hydroxyl radicals in the troposphere, leading to a more rapid decomposition.[4] Compared to the CFCs, a much smaller fraction of HFCs reach the stratosphere. This fact, along with thermodynamic considerations, results in HFCs having a negligible effect on the destruction of the ozone layer.

The photochemistry of HFCs[5,6] and similar hydrochlorofluorocarbons[7−9] has been studied in part to evaluate the potential of these molecules to undergo photoinduced breakdown as well as degradation via radical processes. It has been established that CH_3CFCl_2 excited with three or four quanta in the CH-stretching vibration is substantially more likely to undergo photolysis than when in its vibrational ground state.[8] Because HFCs are replacing CFCs for a variety of applications and are emitted into the atmosphere in large quantities, a complete understanding of their atmospheric photochemistry is desirable. Thus, the intensities of the various CH-stretching overtone transitions of atmospheric HFCs are important in evaluating the likelihood of vibrationally mediated photodissociation. This article considers only the likelihood of overtone excitation; understanding the complete photochemistry might require studies on the effect of overtone excitation on photochemistry.

In the present work, we study the absorption spectroscopy of an ethane-based HFC, 1,1,1,2-tetrafluoroethane, also known as HFC-134a. HFC-134a is already widely in use as a propellant and as a replacement for the refrigerant CF_2Cl_2 (CFC-12). It is approximately five times as abundant as any other HFC in the atmosphere at ground level, with a concentration of 15 ppt in year 2000.[10] HFC-134a is preferred over CFCs because of its lower ozone depletion potential and because it has approximately one-sixth the global warming potential of CF_2Cl_2.[11] HFC-134a is also a good choice for computational studies because of its relatively small size and the fact that it contains only hydrogen and first-row elements.

The spectrum of HFC-134a has been recorded in the infrared region by Edgell et al.,[12] by Nielsen and Halley,[13] and by Papasavva et al.[14] Forster et al.[15] have recently calculated the radiative forcing of HFC-134a using several models. The fundamental region of the infrared spectrum contains several strong CF-stretching peaks between 1000 and 1400 cm^{-1}. There are two major peaks in the CH-stretching region, the A' symmetric (2983 cm^{-1}) and A'' asymmetric (3013 cm^{-1}) stretches. These spectra have been recently assigned with the help of ab initio calculations by Papasavva et al.[14] and by Parra and Zeng.[16] Previous ab initio calculations have focused on the equilibrium geometry, calculations of the barrier to rotation about the C−C bond, and the potential energy and dipole moment as a function of the rotational angle.[16−18] The lowest-energy conformer of HFC-134a has C_s symmetry.

We have measured the room-temperature absorption spectrum of HFC-134a from the fundamental to the fifth CH-stretching overtone region, $\Delta v_{CH} = 1-6$. The spectra of hydrocarbons in the high-energy overtone regions are dominated by CH-stretching vibrational overtones.[19] We have used Fourier transform infrared spectroscopy to measure the $\Delta v_{CH} = 1$

* Address correspondence to this author. E-mail: jthoman@williams.edu.
† Present address: Department of Chemistry, Massachusetts Institute of Technology, Cambridge, Massachusetts 02139.

10.1021/jp058060k CCC: $30.25
Published on Web 06/01/2005

region, dispersive long-path absorption spectroscopy to measure the $\Delta v_{CH} = 2-5$ regions, intracavity laser photoacoustic spectroscopy (ICL-PAS) to measure the $\Delta v_{CH} = 4-6$ regions, and cavity ringdown spectroscopy (CRDS) to measure the $\Delta v_{CH} = 5$ and 6 regions. Measurement of the $\Delta v_{CH} = 5$ region with three different techniques has allowed us to critically evaluate the effects of background subtraction in ICL-PAS and CRDS and to test the accuracy of our measured absolute intensities.

At high levels of vibrational excitation such as those studied here, molecules are well described using a local mode basis because vibrational motion becomes concentrated in individual bonds.[19] The local mode model has been successful in calculating peak positions in CH-stretching vibrational overtone spectra[19−24] and relative intensities and profiles of CH- and OH-stretching overtones.[25−27] Recently, Takahashi et al. have used the local mode model with an ab initio dipole moment function and potential energy surface to study the absolute intensities of CH-stretching fundamental and overtone regions of 1,2-dichloroethane[28] and the OH stretching of some small acids and alcohols.[29] The total intensities of OH-stretching vibrational overtones in methanol, ethanol, and 2-propanol have been studied by Phillips et al. in part to gain a quantitative understanding of their atmospheric reactivity.[30] Donaldson et al.[31] have also used the approach of Kjaergaard et al.[25] to calculate the intensity for the $\Delta v_{OH} = 3$ and 4 transitions in nitric acid. Donaldson et al. have shown that overtone-initiated photochemistry can make a significant contribution to OH radical production in the atmosphere,[32] and they have suggested that CH overtone excitation in certain classes of molecules might also impact their photodissociation rate in the atmosphere.

In the present work, we use a 1D local mode Hamiltonian as well as 2D and 3D harmonically coupled anharmonic oscillator (HCAO) local mode models[27] to calculate the overtone spectrum of HFC-134a. We calculate the dipole moment function ab initio using Hartree−Fock (HF) and B3LYP density functional theories combined with double- and triple-ζ-quality basis sets. We calculate the frequencies and absolute intensities of the CH-stretching and HCH-bending vibrational transitions in the fundamental and overtone regions for comparison to our measured spectrum.

II. Experimental Section

We measure the spectrum of gas-phase HFC-134a (Fluorochem, 99% or Aldrich, 99+%) at room temperature in the CH-stretching regions corresponding to $\Delta v_{CH} = 1-6$. In all experiments, sample pressures are measured using a capacitance manometer.

Conventional Spectroscopy. For the $\Delta v_{CH} = 1$ region, HFC-134a is purified using several freeze−pump−thaw cycles on a vacuum line. We place the sample in a 10-cm cell with cesium iodide windows at a pressure of 5 Torr. The spectrum is recorded from 400 to 4000 cm^{-1} using an average of 64 scans by an FTIR (Nicolet Magna-IR) spectrometer with a resolution of 0.5 cm^{-1}. We subtract a background recorded with an evacuated cell.

For the $\Delta v_{CH} = 2-5$ regions, we use a 4.8-m cell (Infrared Analysis, Inc.), and the spectrum is recorded using a dispersive NIR−vis spectrometer (Perkin-Elmer Lambda 9) with a 1-nm spectral bandwidth. We use pressures of about 100 Torr for the $\Delta v_{CH} = 2$ region and about 800 Torr for the $\Delta v_{CH} = 3-5$ region. We again subtract a background recorded with an evacuated cell.

Intracavity Laser Photoacoustic Spectroscopy. We record the $\Delta v_{CH} = 4-6$ regions using intracavity laser photoacoustic spectroscopy (ICL-PAS). The ICL-PAS apparatus (Otago) has been described previously.[33] Briefly, an argon ion laser (Coherent Innova Sabre) is used to pump either a broadband titanium:sapphire laser (Coherent model 890) to record the $\Delta v_{CH} = 4$ and 5 regions or a dye laser (Coherent model 590) using DCM laser dye (Exciton) to record the $\Delta v_{CH} = 6$ region. The photoacoustic cell contains an electret microphone (Knowles Electronics, Inc. EK3132), and the photoacoustic signal is monitored through a lock-in amplifier (Stanford Research Systems SR830). The titanium:sapphire laser and dye laser are tuned with a three-plate birefringent filter, giving 1-cm^{-1} resolution. We modulate the laser power with an optical chopper (Stanford Research Systems SR540) and reference the lock-in amplifier to the modulation frequency. To normalize the photoacoustic signal, we monitor the laser power with a power meter (Coherent LaserMate-Q) via a digital multimeter (Agilent 34401A). The wavelength calibration of the scans is conducted with a wavemeter (Burleigh WA-1000). The wavelength accuracy is checked by recording a spectrum with a trace amount of water added and comparing to known lines in the HITRAN database.[34] We measure only relative intensities with ICL-PAS.

Cavity Ringdown Spectroscopy. We also record the $\Delta v_{CH} = 5$ and 6 regions using CRDS. Our implementation of CRDS (Williams) has been described in detail[35] and is similar to those described in the literature for measuring vibrational overtone spectra of atmospherically relevant molecules.[36] Briefly, a frequency-doubled 20-Hz, 10-ns pulsed Nd:YAG laser (Spectra-Physics Quanta Ray) is used to pump a tunable dye laser (Spectra-Physics Sirah Cobra-Stretch) using pyridine 2 dye (Exciton) to record the $\Delta v_{CH} = 5$ region and DCM dye (Exciton) to record the $\Delta v_{CH} = 6$ region. A portion of the radiation from the dye laser is directed through spatial filters into the cavity so that pulses of 8−20 μJ impinge on the first of the ringdown mirrors (Los Gatos Research, >99.99% reflective). The intensity of light exiting the cavity is monitored using a photomultiplier tube (Hamamatsu R298) connected to a digital oscilloscope (Gage CompuScope 12100). We fit a single-exponential decay to the intensity of the light exiting the cavity using a least-squares approach. The dye laser is scanned over the regions of interest using a 0.05-nm step size, and each data point is the average of 64 ringdown measurements. Ringdown times, and therefore absorbance measurements, are often said to be independent of the laser power entering the cavity. However, this statement is true only if a single cavity mode, the TEM_{00}, is excited.[37] We observe our ringdown time to be dependent on the power output of our dye laser, indicating that we excite more than a single mode. The effects of this intensity dependence on our baseline will be discussed. Quantitative absorbance information is obtained with CRDS. To calibrate the wavelength of our dye laser, we use the optogalvanic effect to observe well-characterized transitions in neon gas in a glow-discharge lamp.[38]

Using a commercial data analysis package (Igor Pro, Wavemetrics, Inc.), we deconvolute our spectra into a sum of Lorentzian curves and, in the case of the conventional spectroscopies, a linear baseline. Our method of treating the baselines in other techniques is discussed later. We extract the band centers and intensities of individual transitions from the fit. In cases where multiple peaks appear to be superimposed, there is a larger uncertainty in the position of the individual transitions than when the peaks are well separated. In addition, the choice of Lorentzian curves, which have some intensity in the far wings, adds uncertainty to our ability to fit a baseline to the spectrum. The total absorption intensity of a CH-stretching region is determined by trapezoidal integration across the entire region.

The oscillator strength is calculated by[39]

$$f = 2.6935 \times 10^{-9}\,[\mathrm{K}^{-1}\,\mathrm{Torr\ m\ cm}]\,\frac{T}{pl}\int A(\tilde{\nu})\,\mathrm{d}\tilde{\nu} \quad (1)$$

where T is the absolute temperature, p is the pressure of the sample, l is the path length, and $\int A(\tilde{\nu})\,\mathrm{d}\tilde{\nu}$ is the integrated absorbance.

III. Theory and Calculations

The oscillator strength of a vibrational transition within the ground electronic state is given by[39]

$$f_{\mathrm{e}\leftarrow\mathrm{g}} = \frac{4\pi m_{\mathrm{e}}}{3e^2\hbar}\nu_{\mathrm{eg}}\langle \mathrm{e}|\vec{\mu}|\mathrm{g}\rangle^2 \quad (2)$$

where ν_{eg} is the transition frequency and $\langle \mathrm{e}|\vec{\mu}|\mathrm{g}\rangle$ is the transition dipole moment matrix element. The excited- and ground-state vibrational wave functions are e and g, respectively, and surround $\vec{\mu}$, the dipole moment function of the molecule. As usual, m_{e} is the mass of an electron, e is the elementary charge, and $\hbar$ is Planck's constant divided by 2π. We use the dimensionless oscillator strength as a measure of intensity for comparison to our experimental data. We can rewrite eq 2 using the transition wavenumber $\tilde{\nu}_{\mathrm{eg}}$

$$f_{\mathrm{e}\leftarrow\mathrm{g}} = 4.70175 \times 10^{-7}\,[\mathrm{cm\ D}^{-2}]\,\tilde{\nu}_{\mathrm{eg}}|\vec{\mu}_{\mathrm{eg}}|^2 \quad (3)$$

where $\vec{\mu}_{\mathrm{eg}} = \langle \mathrm{e}|\vec{\mu}|\mathrm{g}\rangle$ and the values of the physical constants[40] have been inserted.

We can see from eqs 2 and 3 that in order to calculate the intensity of a transition we need the dipole moment function, the ground- and excited-state vibrational wave functions, and the vibrational transition energy. The vibrational eigenstates and eigenenergies are calculated using a local mode model that is limited to include at most the two CH-stretching modes and the HCH-bending mode. The dipole moment function is obtained from ab initio calculations.

Vibrational Hamiltonian. We initially perform intensity calculations on HFC-134a using a 1D CH-stretching Hamiltonian. We then extend this pure local mode model to 2D and 3D Hamiltonians that include coupling between the CH-stretching modes and between the CH-stretching and HCH-bending local modes, respectively.

We assume that CH-stretching modes may be modeled as Morse oscillators and write our 1D Hamiltonian as

$$H^0_{1\mathrm{D}} = \frac{1}{2}G^0_{11}p_1^2 + D_1(1 - \exp[-a_1q_1])^2 \quad (4)$$

where p_1 is the momentum conjugate to q_1. The internal coordinate q_1 is the displacement from equilibrium of a CH bond length R_1. G_{11} is the Wilson G-matrix element[41] for q_1, evaluated at the equilibrium geometry. D_1 and a_1 are the parameters of the Morse potential. The diagonal matrix elements of $H^0_{1\mathrm{D}}$ are

$$\frac{[H^0_{1\mathrm{D}} - E^0_{|0\rangle}]}{hc} = v\tilde{\omega} - (v^2 + v)\tilde{\omega}x \quad (5)$$

where $\tilde{\omega}$ is the local mode frequency parameter, $\tilde{\omega}x$ is the anharmonicity parameter, $E^0_{|0\rangle}$ is the energy of the vibrational ground state, and v is the vibrational quantum number.

Our 2D Hamiltonian, $H_{2\mathrm{D}}$, is the sum of two equivalent Morse oscillator CH-stretching Hamiltonians with both kinetic and potential energy coupling included in one term. Because we have two equivalent oscillators in HFC-134a, the frequency and anharmonicity parameters for both modes are equal. In this 2D representation, the zeroth-order Hamiltonian is diagonal with matrix elements given by

$$\frac{[H^0_{2\mathrm{D}} - E^0_{|00\rangle}]}{hc} = (v_1 + v_2)\tilde{\omega} - ({v_1}^2 + {v_2}^2 + v_1 + v_2)\tilde{\omega}x \quad (6)$$

where $E^0_{|00\rangle}$ is the energy of the vibrational ground state, and we have the same local mode parameters as in the 1D case. We introduce the harmonic oscillator step-up, $a^\dagger$, and step-down, a, operators[39] to write the coupling between the two oscillators[27] as

$$\frac{H^1_{2\mathrm{D}}}{hc} = -\gamma'(a_1^\dagger a_2 + a_1 a_2^\dagger) \quad (7)$$

The parameter γ' is the intramanifold coupling constant and has been defined previously.[27] γ' contains both kinetic and potential contributions and depends on the masses of the atoms involved, the equilibrium HCH bond angle, and the force constants associated with the stretching of the CH bonds. We can calculate the vibrational energy levels and wave functions by diagonalizing $H^0_{2\mathrm{D}} + H^1_{2\mathrm{D}}$ to obtain what is called the HCAO local mode model.[42] We represent the 2D vibrational wave functions, which are defined by two quantum numbers, v_1 and v_2, with the notation $|v_1v_2\rangle$. Each quantum number represents the number of stretching quanta localized in the bond indicated by the subscript. Basis functions with the same total number of vibrational quanta $\Delta v = v_1 + v_2$ are said to belong to the same manifold. The basis functions are coupled according to $H^1_{2\mathrm{D}}$. Intermanifold couplings occur between states in manifolds that differ in the total number of quanta Δv. In the HCAO model, we neglect the intermanifold coupling because the different manifolds are of substantially different energy and their mixing is small.[25,42−44]

The 3D Hamiltonian, $H_{3\mathrm{D}}$, used in this paper has been described in detail previously for H_2O.[27,45] The HCH symmetric bending vibration is represented by a harmonic oscillator, and the matrix elements of the zeroth-order 3D Hamiltonian are

$$\frac{[H^0_{3\mathrm{D}} - E_{|00\rangle|0\rangle}]}{hc} = (v_1 + v_2)\tilde{\omega}_{\mathrm{s}} + v_3\tilde{\omega}_{\mathrm{b}} - ({v_1}^2 + {v_2}^2 + v_1 + v_2)\tilde{\omega}_{\mathrm{s}}x_{\mathrm{s}} \quad (8)$$

where the basis functions are the product of two Morse oscillator (CH-stretching) wave functions and one harmonic oscillator (HCH-bending) wave function. The basis functions are represented by using the notation $|v_1v_2\rangle|v_3\rangle$, where v_1 and v_2 are vibrational quantum numbers associated with the two CH stretches and v_3 corresponds to the HCH bend.

We again employ the step-up and step-down operators[39] to write stretch−stretch and stretch−bend coupling as

$$\frac{H^1_{3\mathrm{D}}}{hc} = -\gamma'(a_1a_2^\dagger + a_1^\dagger a_2) + fr'(a_1^\dagger a_3 a_3 + a_1 a_3^\dagger a_3^\dagger + a_2^\dagger a_3 a_3 + a_2 a_3^\dagger a_3^\dagger) \quad (9)$$

The first term represents the stretch−stretch coupling, as in the 2D case, and the second term represents the Fermi resonance stretch−bend couplings. The stretch−bend coupling parameter fr' includes both kinetic and potential energy couplings and is defined elsewhere.[27] Diagonalizing $H^0_{3\mathrm{D}} + H^1_{3\mathrm{D}}$ gives the 3D

local mode HCAO model. Because the HCH bending occurs at roughly half the frequency of the CH-stretching fundamental, we introduce the label $\Delta v = v_{CH} + (1/2v_{HCH})$ to denote a transition region or manifold. In the 3D model, states with the same Δv are of similar energy and may couple. States belonging to different manifolds are of substantially different energy, and the coupling between these states is neglected. We neglect states with more than six quanta of stretching or bending motion in our model.

Dipole Moment Function. Because the exact form of the dipole moment function is unknown, we approximate it as a Taylor expansion about the equilibrium geometry. We begin by considering vibration along one stretching coordinate

$$\vec{\mu}(q_1) = \sum_i \vec{\mu}_i q_1^i \tag{10}$$

where the coefficients $\vec{\mu}_i$ are given by the ith derivative of the dipole moment function evaluated at the equilibrium geometry

$$\vec{\mu}_i = \frac{1}{i!}\frac{\partial^i \vec{\mu}}{\partial q_1^i}\bigg|_{eq} \tag{11}$$

To calculate intensities using this 1D dipole moment function and our 1D Hamiltonian (eqs 3 and 5), we need to know the dipole moment as a function of the CH stretch along q_1. We calculate $\vec{\mu}(q_1)$ by displacing q_1 from -0.3 to 0.4 Å in steps of 0.05 Å. We fit a sixth-order polynomial to our 15 points using a least-squares approach. Previously, this fitting routine has been successfully employed to calculate the intensities of the CH-stretching overtone spectra of xylene.[33] Because HFC-134a has two equivalent CH bonds, the total CH-stretching absorption intensity in the 1D model is twice that calculated using a single CH oscillator.

To calculate intensities with our 2D Hamiltonian (eqs 6 and 7), we require a 2D dipole moment function. We allow for displacement from equilibrium in the two CH-stretching coordinates

$$\vec{\mu}(q_1, q_2) = \sum_{i,j} \vec{\mu}_{ij} q_1^i q_2^j \tag{12}$$

where the coefficients $\vec{\mu}_{ij}$ are given by

$$\vec{\mu}_{ij} = \frac{1}{i!j!}\frac{\partial^{i+j} \vec{\mu}}{\partial q_1^i \partial q_2^j}\bigg|_{eq} \tag{13}$$

We calculate the diagonal terms by displacing either q_1 or q_2 from -0.3 to 0.4 Å in steps of 0.05 Å with the other coordinate at equilibrium. We again fit the 15 points to sixth-order polynomials. We note that eq 13 now contains cross terms (i.e., dipole moment derivatives of both coordinates). We calculate the cross terms using a 9×9 grid with both q_1 and q_2 displaced from -0.2 to 0.2 Å in 0.05-Å increments. The 9×9 grid is fit to a series of 9 second-order polynomials in q_1, one at each displaced value of q_2. The coefficients of each order of this series of polynomials are then fitted to another series of second-order polynomials in q_2 to obtain the cross terms. We include only mixed terms up to third order. Our 2D dipole moment function, combined with the eigenfunctions and eigenenergies obtained from our 2D Hamiltonian, allows us to calculate the intensities of transitions predicted by the 2D model.

Upon inclusion of the bending mode in our Hamiltonian, we require a 3D dipole moment function. We extend eq 12 to include dipole moment derivatives of the bending mode

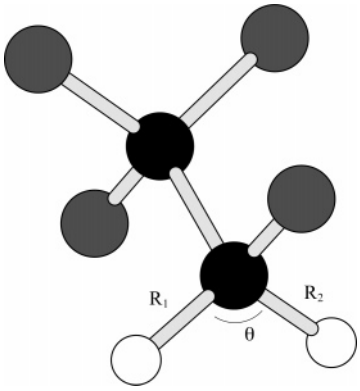

Figure 1. Staggered B3LYP/aug-cc-pVTZ-optimized geometry of 1,1,1,2-tetrafluoroethane (HFC-134a). The molecule has C_s symmetry.

$$\vec{\mu}(q_1, q_2, q_3) = \sum_{i,j,k} \vec{\mu}_{ijk} q_1^i q_2^j q_3^k \tag{14}$$

The coefficients of the expansion are now given by

$$\vec{\mu}_{ijk} = \frac{1}{i!j!k!}\frac{\partial^{i+j+k} \vec{\mu}}{\partial q_1^i \partial q_2^j \partial q_3^k}\bigg|_{eq} \tag{15}$$

where q_3 is the displacement from equilibrium of θ, the HCH bond angle. The dipole derivatives that depend only on the stretching coordinates are calculated as described for the 2D case. A pair of equivalent 2D stretch−bend grids are calculated by displacing the stretching coordinates from -0.2 to 0.2 Å in 0.05-Å increments and displacing the bending coordinate from -20 to 20° in 5° increments. We fit these 2D stretch−bend grids in an identical manner to the 2D grids calculated for the stretch−stretch mixed derivatives. We consider only cross terms involving the displacement from equilibrium of two coordinates. Mixed terms that depend on all three coordinates are ignored. In total, three intersecting 2D grids are calculated: one for the stretch−stretch coupling and one each for the two identical stretch−bend couplings.

Calculations of vibrational transition intensities such as those presented here are approximate in part because of the neglect of vibration−rotation coupling. This problem may be solved by embedding the molecular fixed axes according to the Eckart conditions.[41,46−50] This correction, which has been made for water[27] and H_2S[50] in previous papers, is less important for a larger molecule such as HFC-134a, and we do not perform it here.

We calculate the ab initio-optimized geometry of HFC-134a using the B3LYP level of theory with the Dunning correlation-consistent basis sets aug-cc-pVDZ and aug-cc-pVTZ as well as the Pople split-valence triple-ζ basis set 6-311++G(2d,2p). We also perform an HF/aug-cc-pVTZ calculation. These calculations are performed using Gaussian 03.[51] The B3LYP/aug-cc-pVTZ-optimized geometry has CH bond lengths of 1.0896 Å and an HCH bond angle of 110.60° (Figure 1).

IV. Results and Discussion

The spectrum of HFC-134a in the $\Delta v_{CH} = 1-6$ regions is presented in Figure 2, and the positions and oscillator strengths of the strongest peaks are presented in Table 1. The oscillator strengths are derived from the areas of the spectral features deconvoluted into individual Lorentzian curves. The deconvolution procedure is somewhat subjective. Of course, arbitrarily

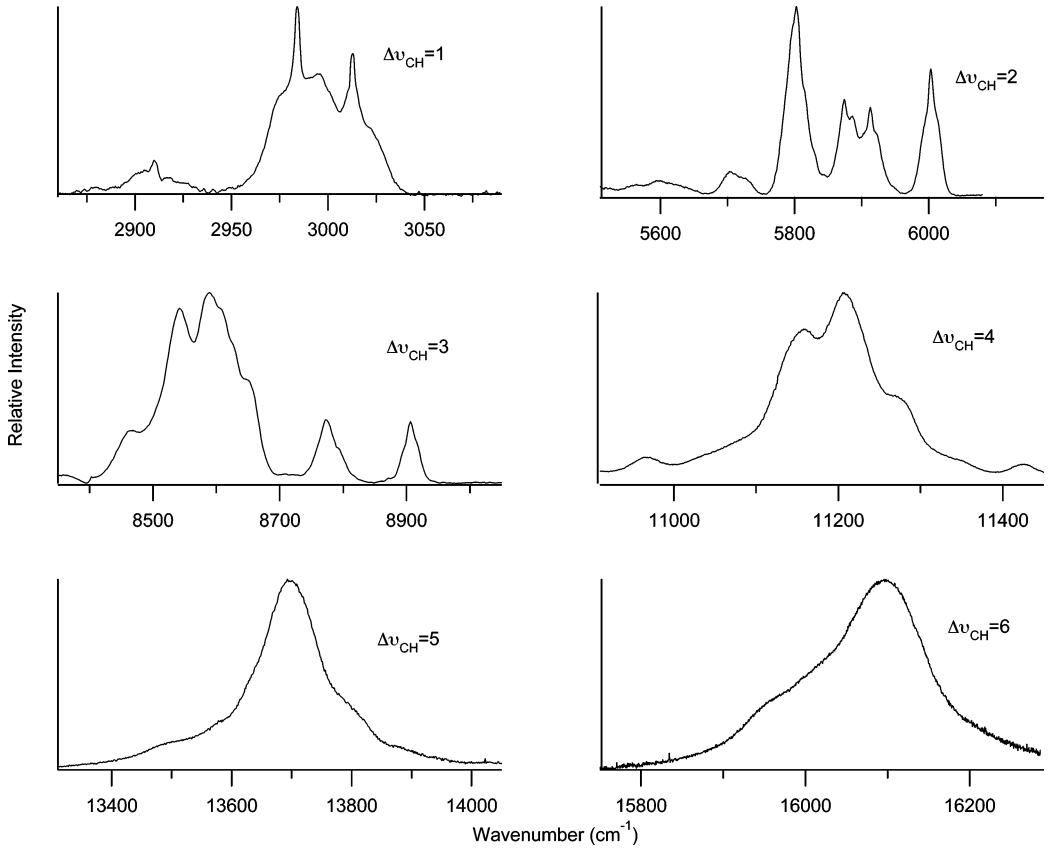

Figure 2. Spectrum of HFC-134a in the $\Delta v_{CH} = 1-6$ regions measured with FTIR spectroscopy ($\Delta v_{CH} = 1$), conventional long-path spectroscopy ($\Delta v_{CH} = 2-3$), and ICL-PAS ($\Delta v_{CH} = 4-6$).

TABLE 1: Observed[a] CH-Stretching Frequencies and Intensities of HFC-134a

Δv_{CH}	$\tilde{\nu}$ (cm^{-1})	f
1[b]	2983.3	3.13×10^{-6}
	3012.8	9.66×10^{-7}
2[c]	5801.2	5.34×10^{-8}
	5877.2	2.27×10^{-8}
	5914.1	2.23×10^{-8}
	6003.8	3.02×10^{-8}
3[c]	8463.9	1.00×10^{-9}
	8538.2	3.94×10^{-9}
	8598.5	7.40×10^{-9}
	8649.8	8.53×10^{-10}
	8775.8	1.11×10^{-9}
	8907.2	9.66×10^{-10}
4	11 147.4,[c] 11 149[d]	2.93×10^{-10c}
	11 209.3,[c] 11 211[d]	6.66×10^{-10c}
	11 276.3,[c] 11 279[d]	5.11×10^{-11c}
5	13 698,[c] 13 697,[d] 13 696[e]	1.06×10^{-10c}, 1.45×10^{-10e}
6	15 987,[d] 15 988[e]	7.31×10^{-12e}
	16 098,[d] 16 102[e]	2.06×10^{-11e}

[a] Deconvoluted from the measured spectrum using a sum of Lorentzian curves. [b] Acquired with FTIR spectroscopy. [c] Acquired with long-path absorption spectroscopy. [d] Acquired with ICL-PAS. [e] Acquired with CRDS.

adding more Lorentzian curves to a deconvolution scheme will improve the quality of the fit to the measured spectrum. We utilize a small number of curves to find the major features in the spectrum for comparison to our model.

We measure the $\Delta v_{CH} = 4$ region with both dispersive long-path spectroscopy and ICL-PAS. The two techniques agree well with respect to the frequencies of the peaks in the region and the shape of the band. ICL-PAS offers a higher signal-to-noise ratio than long path in this region, so we present the ICL-PAS trace in Figure 2. We also present ICL-PAS traces for the $\Delta v_{CH} = 5$ and 6 regions, which have a higher signal-to-noise ratio than the corresponding CRDS spectra (shown in Figures 3 and 4).

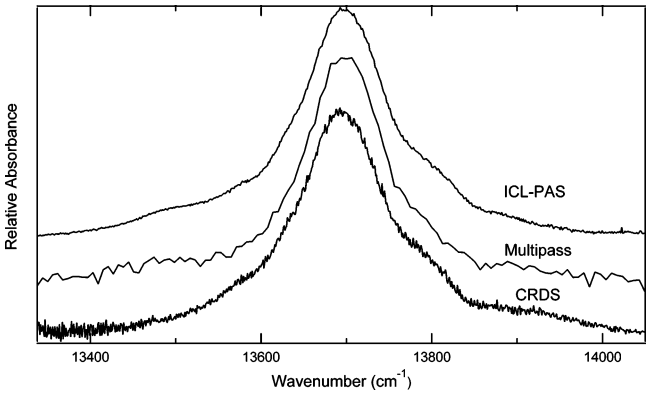

Figure 3. HFC-134a in the $\Delta v_{CH} = 5$ region recorded with CRDS processed using a second-order polynomial baseline (bottom trace), dispersive long-path spectroscopy processed using a linear baseline and a scan of an empty cell (middle trace), and ICL-PAS (top trace). The three traces are offset in the vertical direction and scaled to have equal heights at the maximum absorption.

Experimental Absolute Intensities. The high-overtone transitions measured with CRDS and ICL-PAS have very low intensities. We must therefore account for frequency-dependent effects on our baseline. In CRDS, these may include changing mirror reflectivity or variable dye laser power. We subtract a baseline from our spectrum to compensate for these effects, and the choice of the functional form of the baseline can have a significant impact on the derived intensity of the region. By

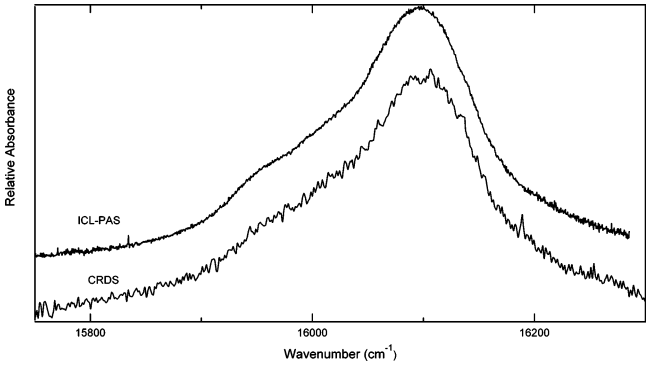

Figure 4. Comparison of the $\Delta v_{CH} = 6$ region of HFC-134a using CRDS (bottom trace) and ICL-PAS. The traces are offset in the vertical direction.

quantifying that impact, we estimate the uncertainty in our measurements of low-intensity transitions. We subtract three different baselines from our CRDS spectrum in the $\Delta v_{CH} = 5$ region: a linear fit, a second-order polynomial, and a scan of an equal pressure of hexafluoroethane (C_2F_6). Hexafluoroethane is used because its geometry is similar to that of 1,1,1,2-tetrafluoroethane but it has no CH bonds to absorb light in the regions of interest. It may therefore be considered to be an approximate model for the light-scattering properties of 1,1,1,2-tetrafluoroethane without the absorbing CH chromophore.

The source of the baseline slope is some combination of factors whose functional form is unknown. The linear fit is the simplest functional form that we can choose as an approximation to the true baseline. Previously, DeMille et al. used a linear fit,[52] but Romanani et al. subtracted a parabolic fit to a CRDS baseline.[37] Because the high overtones are quite broad, the regions of interest are of comparable width to the tuning curves of the laser dyes used to probe them in CRDS. The laser power is therefore lower at the ends of the spectrum than it is in the middle. For this reason, we observe a baseline with upward slopes at either end, making a linear baseline an inappropriate choice. Either the second-order polynomial baseline or the baseline from the hexafluoroethane spectrum does a better job of reproducing this behavior. In contrast to the hexafluoroethane baseline, the second-order polynomial can be fit to the baseline regions on both sides of the feature. A hexafluoroethane spectrum may yield "baseline" values on one side or the other of a spectral feature that do not match the baseline in the sample spectrum. This is because without a perfectly rigid cavity the mirror alignment (and therefore the absorbance) may change slightly each time the cell is evacuated and refilled. This makes recording a background spectrum of any gas or an evacuated cell under the same conditions as the sample spectrum difficult.

We compare three techniques for measuring the $\Delta v_{CH} = 5$ region: CRDS using a second-order polynomial baseline, long path with a linear baseline, and ICL-PAS (Figure 3). The ICL-PAS spectrum is normalized to the laser power and is presented without any further baseline subtraction. The three spectra are in good agreement with respect to the frequency center and shape of the peak, but there are differences in the baseline, leading to different intensities (Table 2). ICL-PAS has the highest signal-to-noise ratio, followed by CRDS and then long-path spectroscopy.

The oscillator strengths derived after subtraction of the second-order polynomial or hexafluoroethane baseline agree with each other and with the results from long-path spectroscopy to within 19% (Table 2). Thus, the uncertainty in absolute

TABLE 2: Total Intensities of the $\Delta v_{CH} = 5$ Region of HFC-134a Using Different Baselines

baseline (technique)	f
linear (long path)	1.16×10^{-10}
linear (CRDS)	1.04×10^{-10}
second-order polynomial (CRDS)	1.12×10^{-10}
hexafluoroethane (CRDS)	1.33×10^{-10}
none subtracted (ICL-PAS; discussed in text)	1.42×10^{-10}

intensity for the $\Delta v_{CH} = 5$ region is at least that large. The correct intensity probably lies somewhere between our various experimental values. For further comparison to theory, we take its oscillator strength to be 1.2×10^{-10}, a result that is consistent with markedly different measurement techniques.

In addition to oscillator strengths derived directly from long path and CRDS for this region, we scale the intensity of our ICL-PAS trace so that the peak absorbance is equal to the CRDS absorbance with the second-order polynomial baseline already subtracted. The ICL-PAS trace can then be integrated to calculate the oscillator strength. This value is presented in Table 2 and is in reasonable agreement with the values derived from CRDS and long path.

For the $\Delta v_{CH} = 6$ region, we compare the shapes of the transitions from CRDS (with a second-order polynomial baseline subtracted) and ICL-PAS in Figure 4. CRDS and ICL-PAS agree well with respect to the appearance of the band and the center frequency. The CRDS spectrum has a few sharp lines and slightly more noise. We scale the intensity information from ICL-PAS in the same manner as for the $\Delta v_{CH} = 5$ region and obtain $f_{ICL-PAS} = 2.27 \times 10^{-11}$, which is about 10% greater than the intensity derived from CRDS ($f_{CRDS} = 2.06 \times 10^{-11}$). Given that $\Delta v_{CH} = 6$ is approximately an order of magnitude less intense than $\Delta v_{CH} = 5$, we expect that our oscillator strength will have a larger uncertainty associated with it than the 19% estimated for the $\Delta v_{CH} = 5$ region. For comparison to theory, we use an oscillator strength of 2.1×10^{-11}. Previously, DeMille et al. have measured the absolute intensity of the $\Delta v_{CH} = 6$ region of several alkanes to within 3%.[52] However, recent measurements[53] by Lewis et al. disagreed with the measurements of DeMille et al. by some 27%, calling the small uncertainty quoted earlier[52] into question.

Overall, we find that measuring the CH-stretching regions with multiple techniques allows us to make some quantitative estimate of the error in our measurements. As implemented in our laboratories, the ICL-PAS spectrum in the $\Delta v_{CH} = 4-6$ regions has a higher signal-to-noise ratio than the corresponding CRDS spectrum and is less affected by a sloping baseline. This is partly because the signal in ICL-PAS is normalized to the laser power but the signal in CRDS is not. The advantage of CRDS is that absolute intensities may be derived from the spectrum. However, the intensities determined are highly dependent on the method used to treat the baseline.

Calculation of Model Parameters. We calculate local mode band positions and intensities using a mixture of experimental and ab initio values. We rely on parameters calculated ab initio where we cannot derive an experimental value. The parameters used in our model are presented in Table 3. Our ab initio-calculated CH bond length agrees with a high-level ab initio study[17] to within the error estimated in that work. Our calculation disagrees with the assumed CH bond length in a microwave experiment[54] by approximately 0.005 Å, though Puzzarini et al.[17] have suggested that the lack of fluorine isotopic substitution data in that study may cause it to disagree somewhat with calculations. Our calculation of the HCH bond angle in HFC-134a disagrees with another microwave study[55] by 1.7°, but the uncertainty quoted in that measurement is 1°.

TABLE 3: Calculated Structural and Local Mode Parameters for HFC-134a

parameter	value
R_{CH}	1.0896 Å[a,b]
θ_{HCH}	110.60°[a]
$\tilde{\omega}_s$	3078.7 cm^{-1}[b,c]
$\tilde{\omega}x_s$	56.53 cm^{-1}[b,c]
γ'	35.5 cm^{-1}[d]
$\tilde{\omega}_b$	1525.9 cm^{-1}[a]
fr'	18.9 cm^{-1}[d]

[a] Calculated ab initio using a B3LYP/aug-cc-pVTZ method. [b] The estimated uncertainty in these parameters is discussed in the text. [c] Calculated from experimental frequencies of the $\Delta v_{CH} = 5$ and 6 transitions. [d] Calculated using an experimental $\tilde{\omega}$ value and ab initio force constants and structural parameters.

Because CH-stretching vibrational overtone intensities are particularly sensitive to the value of $\tilde{\omega}x_s$,[56] it is important to use the most accurate local mode stretching parameters available (i.e., those derived from experiment). The experimental parameters that we derive are taken from the CH-stretching frequencies observed in our experiments. We extract $\tilde{\omega}_s$ and $\tilde{\omega}x_s$, the CH-stretching frequency and anharmonicity, from a Birge−Sponer-type fit[39] of the center frequencies of the $\Delta v_{CH} = 5$ and 6 bands. These regions appear to be the most like pure local modes (i.e., they are the closest to a single absorption peak) and yield values of 3078.7 and 56.53 cm^{-1}, respectively. To estimate the uncertainty in the slope and intercept of this plot, we also perform a Birge−Sponer-type fit to frequency positions of all of the regions measured in this work. For those regions with complicated spectra (i.e., $\Delta v_{CH} = 2-4$), the transition energy is taken from the most intense peak. We estimate the uncertainty in our frequency parameter to be ±22 cm^{-1} and the uncertainty in our anharmonicity parameter to be on the order of ±4 cm^{-1}.

We calculate γ' from our experimental frequency parameter, the ab initio force constants extracted from a fit to our 9 × 9 sretch−stretch grids, and ab initio structural parameters. We obtain a value of 35.5 cm^{-1}. In our model, the value of γ' has no effect on the calculated total intensity of a region; it merely redistributes intensity among different modes of vibration.

There is no simple way of extracting the HCH-bending frequency, $\tilde{\omega}_b$, from our experimental data. We calculate it ab initio to be 1525.9 cm^{-1}. The parameter fr' is calculated to be 18.9 cm^{-1} using the frequency and structural parameters just described as well as the ab initio force constants associated with stretch−bend coupling. We derive our parameters from this mixture of experimental and ab initio methods in the hopes of obtaining a reasonable fit to our data. Ab initio-calculated parameters that include no scaling factors or adjustable parameters do not agree well with our experimental data when calculated using the methods in this paper. We wish to obtain a few local mode parameters from the frequency information in our experiments rather than fit the observed peaks in our spectrum to a model consisting of a number of adjustable local mode parameters (as has been done for another HFC, 1,1,1,2,3,3,3-heptafluoropropane[57]).

Comparison of Computational Methods. The optimized geometry of HFC-134a calculated using the B3LYP/aug-cc-pVTZ method is staggered with C_s symmetry (Figure 1). We calculate the barrier to rotation about the C−C bond in HFC-134a to be 1208 cm^{-1} with this method. Far-infrared spectra obtained by Danti and Wood[58] have shown the barrier height to be 1470 cm^{-1}. However, they assumed inaccurate structural parameters of the molecule, and later calculations by Parra and Zeng[16] using an MP2/6-311++G(3df,3p) method to calculate the single-point energies of MP2/6-311G(d,p)-optimized structures have obtained a barrier of 1303 cm^{-1}. Barriers greater than about 450 cm^{-1} have been shown to be effective in preventing evidence of internal methyl rotation from appearing in room-temperature CH-stretching overtone spectra.[59]

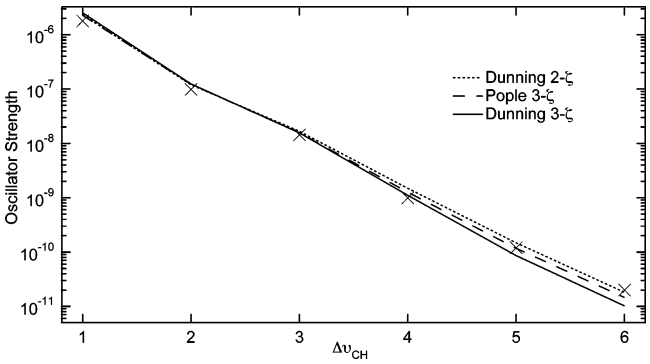

Figure 5. Comparison of experimental total oscillator strength (×) with calculations using the 1D Hamiltonian and the B3LYP/aug-cc-pVDZ (•••), 6-311++G(2d,2p) (- - -), and aug-cc-pVTZ (−) methods.

TABLE 4: Calculated and Observed Total Intensity of CH-Stretching Transitions of HFC-134a

Δv_{CH}	calcd[a]	exptl[b]	calcd/exptl
1	2.49×10^{-6}	1.79×10^{-6}	1.39
2	1.39×10^{-7}	9.90×10^{-8}[c]	1.40
3	1.65×10^{-8}	1.56×10^{-8}[c]	1.06
4	1.12×10^{-9}	9.85×10^{-10}[c]	1.14
5	7.61×10^{-11}	1.16×10^{-10}[c], 1.12×10^{-10}[d]	0.66[c], 0.68[d]
6	8.89×10^{-12}	2.1×10^{-11}[d]	0.42

[a] Using the 3D Hamiltonian and the B3LYP/aug-cc-pVTZ method. [b] Integrated from the measured spectrum. [c] Acquired with dispersive long-path spectroscopy. [d] Acquired with CRDS.

Previously, B3LYP/6-311+G(d,p) and B3LYP/6-311++G-(2d,2p) methods have been successfully employed for the calculation of overtone intensities. B3LYP is a good choice for its reduced computational cost compared to that of higher-level methods such as QCISD and MP3 and its improved accuracy over HF methods.[60] Our calculations on HFC-134a show that HF and B3LYP methods provide similar results for all overtone intensities. B3LYP offers a fundamental intensity that agrees better with experiment, so we use B3LYP results throughout this paper. These conclusions agree with trends that have been previously described[60] but are the first results obtained with an ab initio dipole moment function for a highly fluorinated molecule.

We have chosen three basis sets for our calculations. Recently, Galabov et al. achieved good agreement between experiment and theory for infrared vibrational intensities of a variety of small molecules with the use of Dunning-type triple-ζ basis sets.[61] We calculate intensities using the double-ζ aug-cc-pVDZ, the triple-ζ aug-cc-pVTZ, and the 6-311++G(2d,2p) basis sets. The aug-cc-pVDZ basis set is smaller than 6-311++G(2d,2p), and the aug-cc-pVTZ is the largest of the three.

All three basis sets lead to similar predictions of the intensity of the $\Delta v_{CH} = 1-3$ regions. In the $\Delta v_{CH} = 4$ and 5 regions, 6-311++G(2d,2p) and aug-cc-pVTZ do a substantially better job than aug-cc-pVDZ (Figure 5). Although the aug-cc-pVDZ basis appears to predict the intensity of the $\Delta v_{CH} = 6$ region better, this is almost certainly a comment on the uncertainty in measuring that intensity. As shown in Table 4, the agreement between experiment and theory with the aug-cc-pVTZ basis set, especially at the $\Delta v_{CH} = 3-5$ levels, is excellent. The uncertainty of the calculated intensities increases with increasing change in the vibrational quantum number because of the uncertainty in our Birge−Sponer-type fit. We estimate the

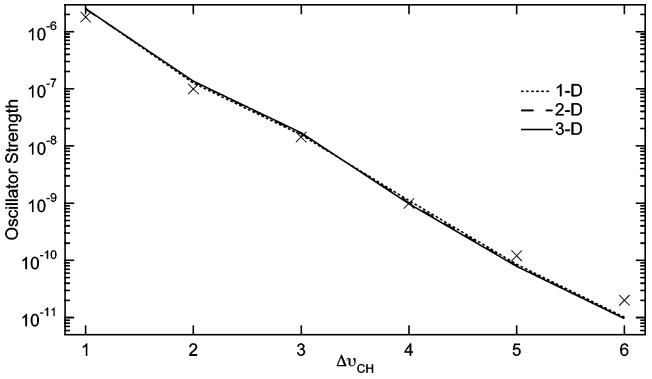

Figure 6. Comparison of experimental total oscillator strength (×) with calculations using the 1D (•••), 2D (- - -), and 3D (−) Hamiltonian using the B3LYP/aug-cc-pVTZ-calculated dipole moment function and local mode parameters from Table 3.

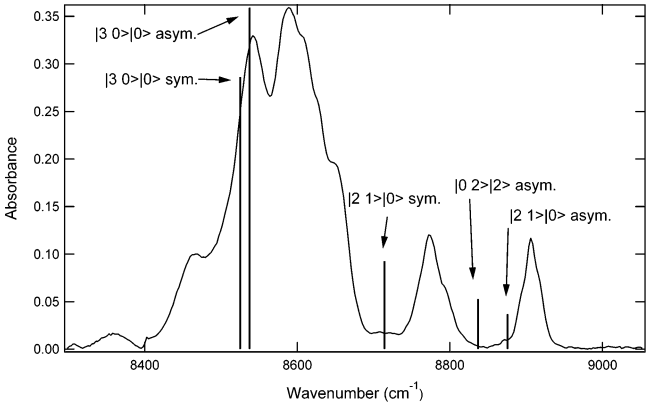

Figure 7. HFC-134a in the $\Delta v_{CH} = 3$ region recorded with dispersive long-path spectroscopy. The 3D B3LYP/aug-cc-pVTZ-calculated transitions are shown as sticks.

uncertainty in intensity due to the uncertainty in $\tilde{\omega}$ and $\tilde{\omega}x$ to be 24% at the $\Delta v_{CH} = 6$ level by performing a 3D aug-cc-pVTZ calculation with the local mode parameters derived from the Birge−Sponer fit to all six measured regions.

Comparison of Model Hamiltonians. Our 1D, 2D, and 3D Hamiltonians yield similar predictions of the total intensity of each region. Most of the intensity is expected to come from the bright CH-stretching state and is therefore accounted for in a model that includes only the CH-stretching vibrations.

Because we wish to determine how well our models explain the structure in each region, we perform calculations using the 2D and 3D models described in section III. Like the 1D model, the 2D and 3D models agree with the experimental total oscillator strengths of each region when used with B3LYP/aug-cc-pVTZ dipole moment functions and local mode parameters from Table 3. The total intensity predictions of the three models are compared in Figure 6. As discussed, there is an uncertainty in the oscillator strengths of the $\Delta v_{CH} = 5$ and 6 regions of greater than 19% based on the uncertainty associated in fitting the baseline. The choice of Hamiltonian has little impact on the calculated total intensity of a region (Figure 6). We do observe a difference in total intensity of about 6% between the 1D and 3D models in the $\Delta v_{CH} = 2$ region. We find that the more complicated Hamiltonians mostly redistribute the intensity over the regions. This indicates that the HCH-bending mode does not significantly influence the intensity of these CH-stretching overtones.

Total Intensity. We observe a general decrease in the total measured intensity of the CH-stretching regions of about an order of magnitude for each successive overtone. This decrease in intensity is consistent with trends previously described in the literature for CH-stretching overtone spectra.[25] Our experimental total intensities agree with our 3D B3LYP/aug-cc-pVTZ calculations to within better than a factor of 2 (Table 4).

We obtain good agreement between our calculated intensities and measured values for all overtones. The fundamental region is often better modeled using a normal mode rather than a truncated local mode picture such as in eqs 8, 9, and 14. However, we are able to calculate the total intensity of each region to within about a factor of 1.4 of the experimental value, except for the CRDS measurement of the intensity in the $\Delta v_{CH} = 6$ region.

Intensity Distribution within CH-Stretching Regions. To visualize how well our vibrational model reproduces the intensity within each CH-stretching overtone, we plot the predictions of the 3D vibrational model using a B3LYP/aug-cc-pVTZ dipole moment function and local mode parameters from Table 3. For the $\Delta v_{CH} = 1-3$ regions of the spectrum, the 3D model does not appear to predict the correct number of important peaks. As an example, the $\Delta v_{CH} = 3$ region is shown in Figure 7.

The frequencies of the individual predicted peaks are not well enough matched with the experimental measurements for definite assignments to be made. The inclusion of additional modes in our Hamiltonian might improve the agreement between experiment and theory with respect to the intensity distribution within each region. Specifically, we might include an A' symmetric CH_2-wagging mode in our Hamiltonian. This mode has been observed in the fundamental region[16] to be close in frequency to the HCH bend that is already included in our model. Additional modes, such as a CC stretch, could also be included.

In the $\Delta v_{CH} = 4-6$ regions, we observe the spectrum to be considerably simpler in appearance than in the lower-energy regions, as is often seen. The $\Delta v_{CH} = 5$ and 6 regions consist of only a single broad peak each, though there may be additional structure present. The overtone spectrum, recorded at room temperature, may be broadened by hot bands, unresolved rotational fine structure, and/or intramolecular vibrational redistribution. Further experiments comparing the structural and temperature dependence of the width of the features are necessary to account for these broad absorptions. Our 3D model predicts two major peaks in each region, separated by less than 2 cm^{-1}.

V. Conclusions

We have recorded the spectrum of HFC-134a in the $\Delta v_{CH} = 1-6$ regions. We have compared the oscillator strengths derived from our experiments to predictions from an anharmonic oscillator local mode model using 1D, 2D, and 3D Hamiltonians. We model one CH stretch, two coupled CH stretches, and two coupled CH stretches with the HCH-bending mode, respectively.

We find that the three model Hamiltonians successfully reproduce the total intensity of each region when used with an ab initio B3LYP/aug-cc-pVTZ dipole moment function. The fact that the quality of the intensity prediction does not significantly improve in the 2D and 3D calculations implies that all of the oscillator strength arises from a bright state that is well described by a pure CH-stretching motion. The addition of extra dimensions in the model serves only to distribute the intensity (and bright-state character) among a set of eigenstates in each CH-stretching region. The inclusion of additional modes in our model might redistribute intensity within CH-stretching regions in a way that better matches the measured spectrum. For the

calculation of total intensity, a 1D local mode model with an ab initio dipole moment function gives quantitative agreement between theory and experiment for our test hydroflurocarbon.

We also find that cavity ringdown spectroscopy and dispersive long-path spectroscopy agree well with respect to the intensity of a transition and that cavity ringdown and intracavity laser photoacoustic spectroscopy agree well with respect to the shape of the transition. The intensities measured for high-overtone regions are particularly dependent on the method of baseline subtraction used.

Acknowledgment. We are grateful to Timothy W. Robinson and Mark H. Schofield for helpful discussions and to Marianna M. Uribe and Jason S. Leith for help with the experiments. We thank an anonymous reviewer for helpful comments. B.G.S. is grateful to the University of Otago for kind hospitality and to the Williams College Center for Environmental Studies for a summer research grant. D.P.S. is grateful to the Foundation for Research, Science and Technology for a Bright Futures scholarship. We acknowledge the University of Otago and the President and Trustees of Williams College for financial support. This material is partly based on work supported by the U.S. National Science Foundation under grant number PHY-9724246.

References and Notes

(1) Wallington, T. J.; Nielsen, O. J. In *Progress and Problems in Atmospheric Chemistry*; Barker, J. R., Ed.; World Scientific: River Edge, NJ, 1995; Chapter 15.
(2) Sukornick, B. *Int. J. Thermophys.* **1982**, *10*, 553.
(3) Molina, M. J.; Rowland, F. S. *Nature* **1974**, *249*, 810.
(4) Chou, C. C.; Milstein, R. J.; Smith, W. S.; Vera Ruiz, H.; Molina, M. J.; Rowland, F. S. *J. Phys. Chem.* **1978**, *82*, 1.
(5) Hasson, A. S.; Moore, C. B.; Smith, I. W. *Int. J. Chem. Kinet.* **1998**, *30*, 541.
(6) Edney, E. O.; Driscoll, D. J. *Int. J. Chem. Kinet.* **1992**, *24*, 1067.
(7) Chen, X.; Marom, R.; Rosenwaks, S.; Bar, I.; Einfeld, T.; Maul, C.; Gericke, K.-H. *J. Chem. Phys.* **2001**, *114*, 9033.
(8) Melchior, A.; Chen, X.; Bar, I.; Rosenwaks, S. *J. Chem. Phys.* **2000**, *112*, 10787.
(9) Einfeld, T.; Maul, C.; Gericke, K.-H.; Maron, R.; Rosenwaks, S.; Bar, I. *J. Chem. Phys.* **2001**, *115*, 6418.
(10) McCulloch, A.; Midgley, P. M.; Ashford, P. *Atmos. Environ.* **2003**, *37*, 889.
(11) McCulloch, A. *J. Fluorine Chem.* **1999**, *100*, 163.
(12) Edgell, F. W.; Riethof, T. R.; Ward, C. J. *J. Mol. Spectrosc.* **1963**, *11*, 92.
(13) Nielsen, J. R.; Halley, C. J. *J. Mol. Spectrosc.* **1965**, *17*, 341.
(14) Papasavva, S.; Tai, S.; Esslinger, A.; Illinger, K. H.; Kenny, J. E. *J. Phys. Chem.* **1995**, *99*, 3438.
(15) Forster, P. M. d. F.; Burkholder, J. B.; Clerbaux, C.; Coheur, P. F.; Dutta, M.; Gohar, L. K.; Hurley, M. D.; Myhre, G.; Portmann, R. W.; Shine, K. P.; Wallington, T. J.; Wuebbles, D. *J. Quant. Spectrosc. Radiat. Transfer* **2005**, *93*, 447.
(16) Parra, R. D.; Zeng, X. C. *J. Phys. Chem. A* **1998**, *102*, 654.
(17) Puzzarini, C.; Dore, L.; Cludi, L.; Cazzoli, G. *Phys. Chem. Chem. Phys.* **2003**, *5*, 1519.
(18) Costa Cabral, B. J.; Guedes, R. C.; Pai-Panandiker, R. S.; Nieto de Castro, C. A. *Phys. Chem. Chem. Phys.* **2001**, *3*, 4200.
(19) Henry, B. R. *Vibrational Spectra and Structure*; Elsevier: Amsterdam, 1981; Vol. 10.
(20) Child, M. S.; Halonen, L. *Adv. Chem. Phys.* **1984**, *57*, 1.
(21) Child, M. S. *Acc. Chem. Res.* **1985**, *18*, 45.
(22) Henry, B. R. *Acc. Chem. Res.* **1987**, *20*, 429.
(23) Ahmed, M. K.; Henry, B. R. *J. Phys. Chem.* **1987**, *91*, 3741.
(24) Ahmed, M. K.; Henry, B. R. *J. Phys. Chem.* **1987**, *91*, 5194.
(25) Kjaergaard, H. G.; Yu, H.; Schattka, B. J.; Henry, B. R.; Tarr, A. W. *J. Chem. Phys.* **1990**, *93*, 6239.
(26) Kjaergaard, H. G.; Henry, B. R. *J. Chem. Phys.* **1992**, *96*, 4841.
(27) Kjaergaard, H. G.; Henry, B. R.; Wei, H.; Lefebvre, S.; Carrington, T. C., Jr.; Sage, M. L. *J. Chem. Phys.* **1994**, *100*, 6228.
(28) Takahashi, K.; Sugaware, M.; Yabushita, S. *J. Phys. Chem. A* **2002**, *106*, 2676.
(29) Takahashi, K.; Sugawara, M.; Yabushita, S. *J. Phys. Chem. A* **2003**, *107*, 11092.
(30) Phillips, J. A.; Orlando, J. J.; Tyndall, G. S.; Vaida, V. *Chem. Phys. Lett.* **1998**, *296*, 377.
(31) Donaldson, D. J.; Orlando, J. J.; Amann, S.; Tyndall, G. S.; Proos, R. J.; Henry, B. R.; Vaida, V. *J. Phys. Chem. A* **1998**, *102*, 5171.
(32) Donaldson, D. J.; Frost, G. J.; Rosenlof, K. H.; Tuck, A. F.; Vaida, V. *Geophys. Res. Lett.* **1997**, *24*, 2651.
(33) Rong, Z.; Kjaergaard, H. G. *J. Phys. Chem. A* **2002**, *106*, 6242.
(34) Rothman, L. S.; Jacquemart, D.; Barbe, A.; Benner, D. C.; Birk, M.; Brown, L. R.; Carleer, M. R.; Chackerian, C., Jr.; Chance, K.; Coudert, L. H.; Dana, V.; Devi, V. M.; Flaud, J.-M.; Gamache, R. R.; Goldman, A.; Hartmann, J.-M.; Jucks, K. W.; Maki, A. G.; Mandin, J.-Y.; Massie, S. T.; Orphal, J.; Perrin, A.; Rinsland, C. P.; Smith, M. A. H.; Tennyson, J.; Tolchenov, R. N.; Toth, R. A.; Auwera, J. V.; Varanasi, P.; Wagner, G. *J. Quant. Spectrosc. Radiat. Transfer*, in press, 2005.
(35) Steeves, A. H. Overtone Spectroscopy of Hydrofluorocarbons: Intensities and Anharmonic Resonances. B.A. Thesis, Williams College, 2002.
(36) Brown, S. S.; Wilson, R. W.; Ravishankara, A. *J. Phys. Chem. A* **2000**, *104*, 4976.
(37) Romanini, D.; Kachanov, A. A.; Stoeckel, F. *Chem. Phys. Lett.* **1997**, *270*, 546.
(38) Nestor, J. R. *Appl. Opt.* **1982**, *21*, 4154.
(39) Atkins, P. *Molecular Quantum Mechanics*, 2nd ed.; Oxford University: Oxford, U.K., 1983.
(40) *CRC Handbook of Chemistry and Physics*, 73rd ed.; Lide, D. R., Ed; Chemical Rubber Company: Boca Raton, FL, 1992.
(41) Wilson, E. B., Jr.; Decius, J.; Cross, P. C. *Molecular Vibrations*; McGraw-Hill: New York, 1955.
(42) Mortensen, O. S.; Henry, B. R.; Mohammadi, M. A. *J. Chem. Phys.* **1981**, *75*, 4800.
(43) Child, M. S.; Lawton, T. R. *Faraday Discuss. Chem. Soc.* **1981**, *71*, 273.
(44) Tamagake, K.; Hyodo, S.; Fujiyama, T. *Bull. Chem. Soc. Jpn.* **1982**, *55*, 1277.
(45) Schofield, D. P.; Kjaergaard, H. G. *Phys. Chem. Chem. Phys.* **2003**, *5*, 3100.
(46) Eckart, C. *Phys. Rev.* **1935**, *47*, 552.
(47) Bunker, P. *Molecular Symmetry and Spectroscopy*; Academic: New York, 1979.
(48) Adler-Golden, S.; Carney, G. *Chem. Phys. Lett.* **1985**, *113*, 582.
(49) Swanton, D.; Bacskay, G.; Hush, N. *J. Chem. Phys.* **1986**, *84*, 5715.
(50) Le Sueur, C. R.; Miller, S.; Tennyson, J.; Sutcliffe, B. T. *Mol. Phys.* **1992**, *76*, 1147.
(51) Frisch, M. J.; Trucks, G. W.; Schlegel, H. B.; Scuseria, G. E.; Robb, M. A.; Cheeseman, J. R.; Montgomery, Jr., J. A.; Vreven, T.; Kudin, K. N.; Burant, J. C.; Millam, J. M.; Iyengar, S. S.; Tomasi, J.; Barone, V.; Mennucci, B.; Cossi, M.; Scalmani, G.; Rega, N.; Petersson, G. A.; Nakatsuji, H.; Hada, M.; Ehara, M.; Toyota, K.; Fukuda, R.; Hasegawa, J.; Ishida, M.; Nakajima, T.; Honda, Y.; Kitao, O.; Nakai, H.; Klene, M.; Li, X.; Knox, J. E.; Hratchian, H. P.; Cross, J. B.; Bakken, V.; Adamo, C.; Jaramillo, J.; Gomperts, R.; Stratmann, R. E.; Yazyev, O.; Austin, A. J.; Cammi, R.; Pomelli, C.; Ochterski, J. W.; Ayala, P. Y.; Morokuma, K.; Voth, G. A.; Salvador, P.; Dannenberg, J. J.; Zakrzewski, V. G.; Dapprich, S.; Daniels, A. D.; Strain, M. C.; Farkas, O.; Malick, D. K.; Rabuck, A. D.; Raghavachari, K.; Foresman, J. B.; Ortiz, J. V.; Cui, Q.; Baboul, A. G.; Clifford, S.; Cioslowski, J.; Stefanov, B. B.; Liu, G.; Liashenko, A.; Piskorz, P.; Komaromi, I.; Martin, R. L.; Fox, D. J.; Keith, T.; Al-Laham, M. A.; Peng, C. Y.; Nanayakkara, A.; Challacombe, M.; Gill, P. M. W.; Johnson, B.; Chen, W.; Wong, M. W.; Gonzalez, C.; Pople, J. A. *Gaussian 03*, Revision B.05; Gaussian, Inc., Wallingford CT, 2004.
(52) DeMille, S.; deLaat, R. H.; Brooks, R. L.; Westwood, N. P. C. *Chem. Phys. Lett.* **2002**, *366*.
(53) Lewis, E. K.; Moehnke, C. J.; Manzanares, C. E. *Chem. Phys. Lett.* **2004**, *394*, 25.
(54) Xu, L.-H.; Andrews, A. M.; Cavanagh, R. R.; Fraser, G. T.; Irikura, K. K.; Lovas, F. J.; Grabow, J.-U.; Stahl, W.; Crawford, M. K.; Smalley, R. J. *J. Phys. Chem. A* **1997**, *101*, 2288.
(55) Ogata, T.; Miki, Y. *J. Mol. Struct.* **1986**, *140*, 49.
(56) Low, G. R.; Kjaergaard, H. G. *J. Chem. Phys.* **1999**, *110*, 9104.
(57) Dübal, H.-R.; Quack, M. *Mol. Phys.* **1984**, *53*, 257.
(58) Danti, A.; Wood, J. L. *J. Chem. Phys.* **1959**, *30*, 582.
(59) Rong, Z.; Howard, D. L.; Kjaergaard, H. G. *J. Phys. Chem. A* **2003**, *107*, 4607.
(60) Kjaergaard, H. G.; Bezar, K. J.; Brooking, K. A. *Mol. Phys.* **1999**, *96*, 1125.
(61) Galabov, B.; Yamaguchi, Y.; Remington, R. B.; Schaeffer, H. F., III. *J. Phys. Chem. A* **2002**, *106*, 819.